Journal of Quantitative Spectroscopy & Radiative Transfer 186 (2017) 243–253

Contents lists available at ScienceDirect

Journal of Quantitative Spectroscopy & Radiative Transfer

journal homepage: www.elsevier.com/locate/jqsrt

The Reference Forward Model (RFM)

Anu Dudhia [a,b,*]

[a] Atmospheric, Oceanic & Planetary Physics, Department of Physics, University of Oxford, Parks Rd, Oxford, United Kingdom
[b] National Centre for Earth Observation, United Kingdom[1]

ARTICLE INFO

Article history:
Received 16 February 2016
Received in revised form
10 June 2016
Accepted 10 June 2016
Available online 23 June 2016

Keywords:
Radiative transfer model
Line-by-line model
Forward model

ABSTRACT

The Reference Forward Model (RFM) is a general purpose line-by-line radiative transfer model, currently supported by the UK National Centre for Earth Observation. This paper outlines the algorithms used by the RFM, focusing on standard calculations of terrestrial atmospheric infrared spectra followed by a brief summary of some additional capabilities and extensions to microwave wavelengths and extraterrestrial atmospheres.

At its most basic level — the 'line-by-line' component — it calculates molecular absorption cross-sections by applying the Voigt lineshape to all transitions up to $\pm 25\ \mathrm{cm}^{-1}$ from line-centre. Alternatively, absorptions can be directly interpolated from various forms of tabulated data.

These cross-sections are then used to construct infrared radiance or transmittance spectra for ray paths through homogeneous cells, plane-parallel or circular atmospheres.

At a higher level, the RFM can apply instrumental convolutions to simulate measurements from Fourier transform spectrometers. It can also calculate Jacobian spectra and so act as a stand-alone forward model within a retrieval scheme.

The RFM is designed for robustness, flexibility and ease-of-use (particularly by the non-expert), and no claims are made for superior accuracy, or indeed novelty, compared to other line-by-line codes. Its main limitations at present are a lack of scattering and simplified modelling of surface reflectance and line-mixing.

1. Introduction

The Reference Forward Model (RFM) was originally developed in the mid-1990s under an ESA contract to provide reference spectra for the MIPAS [12] limb-viewing infrared Fourier-transform spectrometer on the Envisat satellite. It started as a recoded version of GENLN2 [9] and, at its core, it still uses the GENLN2 approach to the line-by-line summation but its capabilities have gradually been extended to include a wide range of radiative transfer applications, from microwave to infrared wavelengths (see Table 1), and the ability to simulate satellite, aircraft/balloon or ground observations. Although the RFM does not include any scattering processes, it can still be used to compute molecular absorption at shorter wavelengths.

The RFM has featured in several model intercomparison exercises [14,33,31,4,27]. It has been used to provide the 'clear sky' component within scattering models [11,5], to generate monochromatic absorption coefficients for fast forward models [8,2,32] and as the actual forward model within retrieval schemes [15,35]. It has also been used to model atmospheres of other planets [20,19].

The code itself is designed for portability and robustness: written in (almost) standard Fortran77 and with input/output mostly via text files. It is also designed to be used as a 'black box' requiring the minimum of inputs and sensible defaults.

* Correspondence address: Atmospheric, Oceanic & Planetary Physics, Department of Physics, University of Oxford, Parks Rd, Oxford, United Kingdom.
E-mail address: anu.dudhia@physics.ox.ac.uk
[1] www.nceo.ac.uk

http://dx.doi.org/10.1016/j.jqsrt.2016.06.018
0022-4073/

Table 1
Summary of RFM features.

Description	Details
General capabilities	
Satellite, aircraft/balloon, ground-based geometries	
Selection of specific isotopomers and vibration levels	
Homogeneous, plane-parallel or circular atmospheres	
Specific options	
Radiance, transmittance, etc. output spectra	Section 6.1
Aerosol extinction	Section 6.2
Molecular continua	Section 6.3
CO_2 line mixing	Section 6.4
CO_2 χ factor	Section 6.5
Collision Induced absorption	Section 6.6
Generate/use look-up tables of absorption cross-section	Section 6.7
Surface parameters	Section 6.8
Instrument line shape convolution	Section 6.9
Field-of-view convolution	Section 6.10
Jacobian (weighting function) spectra	Section 6.11
Horizontal atmospheric structure	Section 6.12
Non-LTE calculations	Section 6.13
Linear-in-tau layer emission	Section 6.14
Flux calculations and matrices	Section 6.15
Rayleigh extinction	Section 6.16
Specific applications	
Microwave spectra	Section 7.1
Extraterrestrial atmospheres	Section 7.2
Visible and ultraviolet spectra	Section 7.3

The aim of this paper is to outline some the basic algorithms used within the RFM at a level of detail allowing it to be compared with other models and to help in the interpretation of results. The source code is, in any case, available and clearly commented and more technical details are available on-line in the Software User's Manual which can be found on the RFM web-site [7].

The last major update of the RFM was v4.30 (September 2013), which made it compatible with the HITRAN 2012 database [25]. Subsequent versions (the latest is v4.34) have contained bug fixes and minor new features. The maintenance and development of the RFM are currently supported by the National Centre for Earth Observation. The code is free and can be obtained by contacting the author.

The main part of this paper describes the four basic structural components of the RFM which, in sequence, are

1. Defining the Calculation
2. Ray-tracing, including calculation of Curtis–Godson integrals
3. Calculation of absorption coefficients (including the line-by-line component)
4. Radiative transfer

These are followed by sections describing some of the optional features, and specific applications of the RFM.

2. Defining the calculation

The RFM is controlled by a text driver file in which the user specifies, as a minimum,

1. the type of output spectra required (e.g., radiance, transmittance)
2. the range and resolution of the output spectra
3. the list of absorbing species (or let the RFM select these itself)
4. the atmospheric profile
5. the viewing geometry
6. the sources of spectroscopic data.

Other inputs may also be required depending on the selected options. For example, an instrument line shape if convolved output spectra are required (Section 6.9).

The first three items are self-explanatory, the others are explained in more detail in the following.

2.1. Atmospheric profile

The RFM requires vertical profiles of temperature, pressure, and volume mixing ratios (VMRs) of all required absorbing molecules (also aerosol, Section 6.2) on a common set of (geometric) altitude levels. Strictly, these are profiles of 'mole fraction' rather than VMR, i.e., the ratio of the number of molecules of a particular species to the *total* number of air molecules but 'VMR' will be used here as a convenient abbreviation (the distinction is only important for species with relatively high concentrations). As an aside, no special distinction is made for water vapour: 'air' here is 'moist air' rather than 'dry air'. It is not necessary to specify *every* molecular component of the atmosphere; the complement of the mole fraction is assumed to be made up of non-absorbing molecules. The surface is assumed to be located at the lowest altitude level, not necessarily 0 km.

By default, a 1-D atmosphere is assumed, i.e., vertical structure only (see Section 6.12 for a 2-D atmosphere).

The user-defined altitude grid is also used for the internal representation of the atmosphere: n profile levels defining $n-1$ atmospheric layers, which in turn defines the physical thickness of the equivalent homogeneous path segments used for spectroscopic calculations and the radiative transfer. The layering can have a significant effect on the accuracy: particularly the assumption that the layer emits at a uniform temperature irrespective of its optical thickness (see Section 6.14). For a typical satellite application, 20–30 layers are usually adequate, with thickness varying from 1 km near the surface to 10 km or more in the mesosphere.

2.2. Viewing geometry

The definition of viewing geometry depends on which of three possible representations of the atmosphere are used. In order of increasing complexity these are:

1. Homogeneous
2. Planar
3. Circular

The homogeneous case, suitable for representing lab measurements or horizontal paths in the free atmosphere, is trivial and, apart from temperature, pressure and

composition, the only additional parameter required to define the 'view' is the path length.

The planar representation treats the atmosphere as a set of horizontal layers ('plane parallel' assumption). The viewing direction is specified by $\sec\theta$ (equivalent to an 'air mass factor'), where θ is the angle with respect to the vertical. Provided that θ represents the viewing angle at the surface rather than the satellite, this generally provides an acceptable simulation for nadir-viewing instruments, at least for $\sec\theta \lesssim 2$.

The circular atmosphere is the most general case, allowing for the curvature of the earth, refraction and field-of-view convolution (Section 6.10). The curvature is assumed fixed over the path length, i.e., profile levels forming concentric circles in the viewing plane. Viewing directions can be specified either as tangent heights (for limb-viewing) or elevation angles α relative to the observer horizontal (suitable for geometries which intersect the surface or upward views from within the atmosphere), in which case the observation altitude is also required. In principle, nadir-views of the circular ($\alpha = -90^\circ$) and planar ($\theta = 0$) atmospheres are identical, refraction and curvature having no effect; however small differences arise from the different path integration methods (Section 3).

2.3. Spectroscopic data

Depending on the molecule, spectroscopic data are obtained either from database of line parameters or from cross-section files containing direct tabulations of spectral absorption coefficient.

The HITRAN 2012 line database [25] consists of text records, one for each transition, for 47 different molecules, arranged in order of increasing wavenumber. Accessing this would be rather slow so, instead, the RFM uses its own binary, direct-access conversion of the data. The RFM cross-section data are basically the same as the HITRAN cross-section format but with the addition of a header record. Look-Up Tables (LUTs) can also be used as an alternative to either line or cross-section data (Section 6.7).

The RFM web-site [7] includes Fortran software to convert HITRAN line and cross-section data to RFM format, also to convert GEISA [16] line and cross-section data to the equivalent HITRAN format, and thence to RFM format.

Internally the RFM uses a numerical code to identify each molecule, with numbers 1–47 matching the HITRAN assignments, and numbers ≥ 100 for cross-section molecules (see RFM web-site [7] for full list). Certain molecules, e.g., SF_6, can be represented either by line parameters (HITRAN/RFM code 30) or by cross-section data (RFM code 103) but, to avoid double-counting, the RFM does not allow a mixture of both.

3. Path integrals

For the multilayer (planar and circular) atmospheres, each viewing direction defines a ray path, and the intersection of each of these ray paths with the profile levels defines *path segments*, with a separate path segment allocated for each absorbing species. Thus an upward view

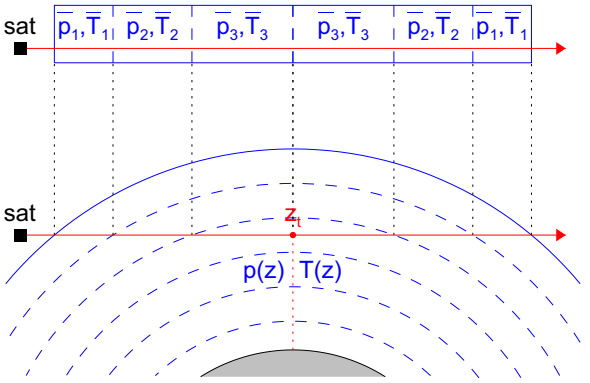

Fig. 1. Construction of path segments for a limb-viewing geometry. The lower panel shows the ray path with (refracted) tangent height z_t through a layered atmosphere. The upper part of the diagram shows the equivalent set of homogeneous paths, used to approximate the atmospheric ray path. The $\overline{p}_i, \overline{T}_i$ are the Curtis–Godson equivalent pressures and temperatures for the segment of the ray path through the corresponding layer i of the atmosphere (assumed symmetric about the tangent point).

from the surface through an atmosphere specified at n altitude levels with m absorbing species will have $m(n-1)$ path segments. For limb-viewing, the tangent point itself also serves to delimit path segments (Fig. 1). The inhomogeneous atmospheric layer within each path segment is then represented by an equivalent homogeneous path, assumed to have the same absorption and emission characteristics.

3.1. Curtis–Godson integrals

The optical thickness χ_{seg} of an absorber with volume mixing ratio v within an atmospheric path segment is given by

$$\chi_{\text{seg}} = \int_{\text{seg}} k(p,T,e) v \rho \, \mathrm{d}s \tag{1}$$

where k is the absorption coefficient which is in general a function of pressure p, temperature T and partial pressure e, ρ is the (molecular) air density and s the distance along the path. k, and therefore χ_{seg} also have spectral dependence but that does not influence the following.

The Curtis–Godson (CG) approximation (see, for example, [24]) is the assumption that this atmospheric path segment has the same optical thickness as a homogeneous path containing the same absorber amount characterised by the absorber-weighted mean values of p, T and e:

$$\chi_{\text{seg}} \simeq k(\overline{p}, \overline{T}, \overline{e}) u \tag{2}$$

where

$$u = \int_{\text{seg}} v \rho \, \mathrm{d}s \tag{3}$$

$$\overline{p} = \frac{1}{u} \int_{\text{seg}} p v \rho \, \mathrm{d}s \tag{4}$$

$$\overline{T} = \frac{1}{u}\int_{\text{seg}} T v \rho \, \mathrm{d}s \tag{5}$$

$$\overline{e} = \frac{1}{u}\int_{\text{seg}} p v^2 \rho \, \mathrm{d}s \tag{6}$$

For a planar atmosphere, converting to pressure as the vertical coordinate, these integrals can be solved analytically and, since secθ simply acts to scale u, do not depend on viewing angle.

For a circular atmosphere, a numerical integration along the path coordinate is required and this is most conveniently combined with the ray-tracing.

3.2. Ray tracing

Applying Snell's Law to a circularly symmetric atmosphere, it can be shown (e.g., [24]) that a refracted rays follows:

$$nr \sin\theta = r_g \tag{7}$$

where n is the refractive index, r is the radial distance, θ is the angle of the path to the local vertical (see Fig. 2) and r_g is a constant defining the path. By considering the situation at the satellite, where $n=1$, it can be seen that r_g represents the geometric (i.e., unrefracted) projection of the tangent point from the satellite.

Eq. (7) can be used (see, for example, [24]) to derive the variation in (r,θ) along the path coordinate, s:

$$\frac{\mathrm{d}r\cos\theta}{\mathrm{d}s} = 1 + \frac{r}{n}\left(\frac{\mathrm{d}n}{\mathrm{d}r}\right)\sin^2\theta \tag{8}$$

This allows a numerical integration of ds within each atmospheric layer, whilst also computing the CG integrals for each absorber.

3.3. Refractive index

It is convenient to define refractive index n in terms of refractivity $N = n-1$. The RFM uses a slight modification [17] of the original Edlén formula:

$$N = 10^{-8}\left(\frac{\rho}{\rho_{\text{ref}}}\right) \times \left[8342.54 + \frac{2\,406\,147}{(130-(1/\lambda)^2)} + \frac{15998}{(38.9-(1/\lambda)^2)}\right] \tag{9}$$

where λ is the wavelength in μm (so $\lambda = 10^4/\nu$ where ν is the wavenumber in cm^{-1}) and ρ_{ref} is the air density evaluated at standard pressure and $T = 15$ °C.

For wavelengths longer than 1 μm (i.e., infrared and microwave) this expression has an almost a constant value $N \simeq 2.7\times10^{-4}(\rho/\rho_{\text{ref}})$. No dependence on water-vapour is included, although this can be significant in the microwave region.

At the tangent point, $\theta = 90°$, so Eq. (7) can be rearranged to show that the reduction in tangent height due to refraction is

$$r_g - r = Nr \tag{10}$$

which corresponds to about 1.7 km at the surface, and decreases with altitude in proportion to air density.

4. Spectral calculations

The next step is to calculate the spectral absorption coefficient for each path segment. It is noted, however, that there will often be path segments with similar if not identical CG pressures and temperatures (although differing absorber amounts), associated with different ray-paths passing through the same atmospheric layer (for example, the inherent symmetry associated with limb-viewing Fig. 1). Computation time can be saved by identifying such cases and only performing explicit spectral calculations for a subset of path segments.

4.1. Line-by-line calculation

For molecules with transition parameters (see Table 2) listed in the HITRAN database, a line-by-line calculation is performed. At wavenumber ν, the absorption coefficient is obtained by summing the contributions of all local transitions of the molecule

$$k(\nu,p,T,e) = \sum_i S_i(T) f(\nu-\nu_{0i},p,T,e,\gamma_{\text{air}},\gamma_{\text{self}},n,\delta) \tag{11}$$

where S_i is the intensity, ν_{0i} the position and f_i the Voigt [34] lineshape of line i. The Voigt lineshape itself is a function of the CG parameters p,T,e (Eqs. (4)–(6)), and $\gamma_{\text{air}},\gamma_{\text{self}},n,\delta$ are additional HITRAN parameters defined in Table 2 (in practice, partial pressure e and self-broadening γ_{self} are only significant for water-vapour in the lower troposphere).

The HITRAN line intensities are listed for a reference temperature of $T_{\text{ref}} = 296$ K and are modified for arbitrary temperature T using the standard formulation (see, for example, Appendix A.2 of Rothman et al. [26])

$$\frac{S(T)}{S(T_{\text{ref}})} = \frac{Q(T_{\text{ref}})}{Q(T)}\left(\frac{\exp(-hcE_i^L/kT)}{\exp(-hcE_i^L/kT_{\text{ref}})}\right)\left(\frac{1-\exp(-hc\nu_0/kT)}{1-\exp(-hc\nu_0/kT_{\text{ref}})}\right) \tag{12}$$

where Q is the 'Partition Function' and h,c,k are, respectively, the Planck constant, the speed of light and the Boltzmann constant. The second term on the r.h.s. is the ratio of the Boltzmann populations, dependent upon the energy of the lower state E^L (given in the HITRAN database) and the final term the effect of stimulated emission. The Partition Functions $Q(T)$ are obtained from pre-tabulated data [13] at 25 K intervals using the recommended 4th-order Lagrangian interpolation.

4.2. Molecular cross-section data

A number of heavy molecules (e.g., N_2O_5, CFCs) have dense spectral structure which is not separable into individual transitions under normal atmospheric conditions. For these, the absorption cross-sections $k(\nu,p,T)$ are available (e.g., on the HITRAN and GEISA web-sites) as files containing collections of tabulated spectra at different (p, T) conditions, corresponding to direct lab measurements.

In principle these are simpler to use than HITRAN lines, because the tabulation is only at a discrete set of (p,T) values which do not, generally, form a rectangular grid, differences can arise between different radiative transfer models simply due to the chosen interpolation scheme.

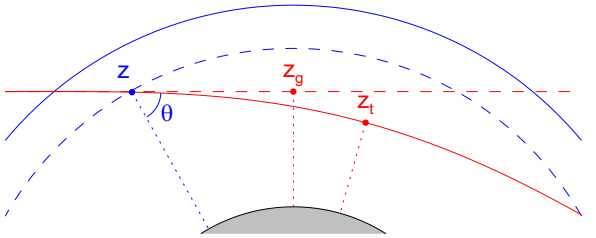

Fig. 2. Effect of refraction on a ray-path (solid red line) compared to the projected geometric path (dashed line) for a satellite off to the left of the picture. z_g represents the *geometric* tangent altitude and z_t the *refracted* tangent altitude. At some arbitrary altitude z along the ray, the path direction is defined by the angle θ relative to the local vertical. As well as increasing the tangent pressure, refraction also acts to lengthen the ray path through the atmosphere, further increasing the optical thickness. (For interpretation of the references to color in this figure caption, the reader is referred to the web version of this paper.)

Table 2
List of HITRAN parameters used by the RFM.

Symbol	Parameter	Units
ν_0	Transition wavenumber	cm^{-1}
S	Line intensity	$cm^{-1}/(mol\ cm^{-2})$
γ_{air}	Air-broadened width	$cm^{-1}\ atm^{-1}$
γ_{self}	Self-broadened width	$cm^{-1}\ atm^{-1}$
E^L	Lower-state energy	cm^{-1}
n	Temperature dependence of air width	
δ	Pressure shift	$cm^{-1}\ atm^{-1}$
	Vibrational quanta (only required for non-LTE calculations, Section 6.13)	
	Local quanta (only required for line-mixing Section 6.4)	

The RFM interpolates using triangulation assuming a linear dependence in both p and T axes. No extrapolation is performed; any points outside the triangulated area are assigned the value at the closest boundary (see Fig. 3).

It should also be noted that, being directly derived from measured spectra, the low pressure data is often dominated by noise which is nevertheless treated as real spectral structure.

4.3. Spectral grids

With any line-by-line calculation there is the practical issue of establishing which lines from the HITRAN database are to be included in the summation of Eq. (11), and at what spectral sampling. These determine the total number of Voigt line shape calculations required, which is usually the major component of the overall computation time. The RFM approach, inherited from GENLN2, is as follows.

The user defines the spectral resolution of the calculations, known as the 'finemesh grid'. This would generally be determined by the resolution required to capture the 'area', if not the detailed structure, of atmospheric emission features. At high altitudes, this is set by the Doppler broadening of atmospheric lines which limit the half-width to around 0.001 cm^{-1} in the mid-infrared. Therefore a sampling of 0.0005 cm^{-1} is generally recommended for limb-viewing, although often relaxed to 0.001 cm^{-1} for nadir-viewing where the radiance contrast with the background is smaller.

The RFM divides the required spectral range into 1 cm^{-1} wide intervals (the 'widemesh grid') and then applies the following rules (Fig. 4)

1. Local lines: any line centred within a 1 cm^{-1} grid interval, or in the adjacent interval, the lineshape $f(\nu_j-\nu_0)$ is evaluated at every finemesh grid point ν_j.
2. Remote lines: any line centred outside these three 1 cm^{-1} intervals, but within 25 cm^{-1} is evaluated at just 3 points: the boundaries and the mid-point of the central 1 cm^{-1} interval.
3. Any line centred beyond 25 cm^{-1} is ignored (although continuum contributions may still be included Section 6.3)

This is implemented as a first pass reading through the HITRAN database evaluating, summing and storing line absorption coefficients of all remote lines at 3 points (edges and mid-point) of each 1 cm^{-1} interval.

A second pass is then made stepping through each 1 cm^{-1} interval in turn. For each interval the remote line contributions are interpolated to the finemesh grid using an inverse quadratic (simulating the $1/\nu^2$ dependence of pressure-broadened lineshapes) and, reading through the HITRAN database for a second time, local line contributions are evaluated and summed also on the finemesh grid. Other sources of spectroscopic data, such as pre-tabulated cross-sections and continua (Section 6.3), are also interpolated to the finemesh grid on this pass.

One useful feature of this approach is that the calculated spectral values are independent of the specified spectral range.

5. Radiative transfer

5.1. Radiative transfer equation

The monochromatic radiance reaching the satellite from a limb path is given by the radiative transfer equation

$$L = \int_{limb}^{sat} B\left(\frac{d\tau}{ds}\right) ds + B_0\tau_{atm} \tag{13}$$

where the integration is evaluated along a path s from space through the atmosphere to the satellite, τ_{atm} is the net atmospheric transmittance and B_0 is the Planck function for cold space (significant only in the microwave region).

For paths which intersect the earth's surface, emissivity ϵ, specular reflection is assumed for simplicity (although see point 4 in the Conclusions)

$$L = \int_{sfc}^{sat} B\left(\frac{d\tau}{ds}\right) ds + \epsilon B_{sfc}\tau_{atm} + (1-\epsilon)\tau_{atm}\int_{spc}^{sfc} B\left(\frac{d\tau}{ds}\right) ds + (1-\epsilon)B_0\tau_{atm}^2 \tag{14}$$

where the first term is evaluated upward from the surface to space, the second term represents the surface radiance, the third term, evaluated from space down to the surface,

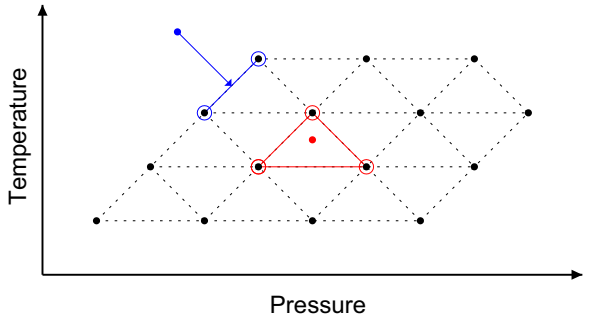

Fig. 3. Diagram showing the method used to interpolate irregularly gridded (p,T) coordinates of tabulated cross section data. The black dots represent the set of (p,T) coordinates of the tabulated data and dotted lines the fitted triangulation grid. If a required (p,T) coordinate lies within the grid (red) the value is interpolated from the three tabulated points which form the local triangle. If the point lies outside the grid (blue), its value is obtained at the closest grid boundary, point (shown by arrow) from the two adjacent tabulated points. (For interpretation of the references to color in this figure caption, the reader is referred to the web version of this paper.)

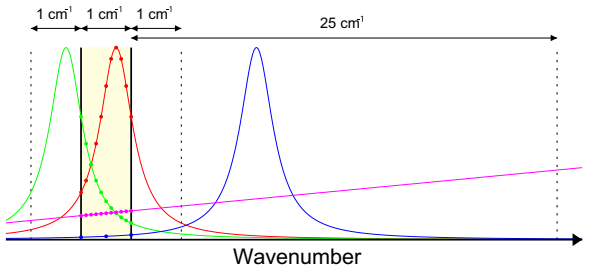

Fig. 4. RFM spectral grids. To calculate the net absorption coefficient within each 1 cm^{-1} interval (pale yellow region) the RFM evaluates the contributions of any local lines centred within this region (red) or adjacent intervals (green) at the resolution of the fine grid (shown by dots). Remote lines, centred outside 1 cm^{-1} but within 25 cm^{-1} of either edge of the interval (blue), are evaluated at just three points within the interval. Any continuum or cross-section data (purple) is simply interpolated to the fine grid. Lines centred outside 25 cm^{-1} are ignored — assumed to be incorporated into the continuum terms. (For interpretation of the references to color in this figure caption, the reader is referred to the web version of this paper.)

is the reflected component and the final term the (usually negligible) reflected cold space contribution. Since specular reflection is assumed, the downward and upward paths are identical. For 'black' surfaces with $\epsilon = 1$ (usually a reasonable approximation for the ocean in the infrared), only the first two terms are evaluated and Eq. (14) reduces to the same form as Eq. (13) with B_{sfc} replacing B_0.

Transmittance is related to optical thickness χ by $\tau = \exp(-\chi)$, hence $\mathrm{d}\tau = -\tau\,\mathrm{d}\chi$, so the integrals can be evaluated numerically as a summation over ray path segments

$$L \simeq \sum_i \overline{B}_i \tau_i \left(1 - \exp(-\chi_i)\right) \tag{15}$$

where i denotes segment number, $\overline{B}_i$ is the effective Planck function, τ_i is the transmittance from the satellite to the near end of the segment, χ_i is the segment optical thickness. These terms are described in more detail in the following sections.

5.2. Optical thickness χ_i

The (monochromatic) optical thickness χ_i of a path segment is the sum of the optical thicknesses χ_{gi} of individual absorbing species g

$$\chi_i = \sum_g \chi_{gi} \tag{16}$$

$$\chi_i = \sum k_{gi} u_{gi} \tag{17}$$

where the absorption coefficients k_{gi} are calculated according to Eq. (11), and absorber amounts u_{gi} according to Eq. (3).

5.3. Transmittance τ_i

The transmittance in Eq. (15) is the transmittance from the observer to the 'near' edge of the segment. Denoting segment $i=1$ as the closest path segment to the satellite (hence $\tau_1 = 1$)

$$\tau_i = \exp\left(-\sum_{j=1}^{i-1} \chi_j\right) \tag{18}$$

where χ_j (Eq. 16) is the optical thickness of each segment between segment i and the satellite.

5.4. Source function $\overline{B}_i$

The source function of a segment is taken as the absorption-weighted mean of the Planck functions evaluated for each absorber CG temperature:

$$\overline{B}_i = \left(\frac{1}{\sum_g \chi_{gi}}\right) \sum_g B(T_{gi}) \chi_{gi} \tag{19}$$

where T_{gi} are the CG temperatures (Eq. (5)). This representation of $\overline{B}_i$ broadly follows the smooth spectral variation of the Planck function itself, but with some small superimposed structure reflecting the variation between the different absorber $B(T_{gi})$ values associated with different absorber distributions within the layer. See Section 6.14 for an alternative representation.

6. Specific options

6.1. Output spectra

Internally the RFM calculates spectra of optical depth χ, transmittance τ and radiance L broadly related as

$$\tau = \exp(-\chi) \tag{20}$$

$$L = \int B\,\mathrm{d}\tau \tag{21}$$

These can be directly output or converted to related quantities such as absorption a, brightness temperature T_{BB} and Rayleigh–Jeans temperature T_{RJ}.

$$a = 1 - \tau \tag{22}$$

$$T_{BB} = \frac{c_2 \nu}{\ln(1 + c_1 \nu^3 / L)} \quad (23)$$

$$T_{RJ} = \frac{L}{2kc\nu^2} \quad (24)$$

where $c_1 = 2hc^2$, $c_2 = hc/k$ are the radiation constants. Note that T_{BB} follows from the formal inversion of the Planck function

$$B = \frac{c_1 \nu^3}{\exp(c_2 \nu / T_{BB}) - 1} \quad (25)$$

and is typically used to represent infrared nadir spectra, while the Rayleigh–Jeans temperature is a linear scaling of the radiance usually used to represent microwave radiances. The two converge when the argument of the exponent in Eq. (25) (or of the logarithm in Eq. (22)) is $\ll 1$ but the RFM always evaluates them differently.

6.2. Aerosol

The RFM does not model scattering (yet, see point 3 in the Conclusions) so can only represent the absorption component of aerosol extinction. The vertical distribution of aerosol (or cloud) is represented by an extinction profile σ_{ext} (km^{-1}) with the spectral dependence provided as an absorption cross-section file. Internally, extinction is scaled by air density ρ and thereafter treated as a VMR v_{ext}. By analogy with Eqs. (2) and (3), the aerosol optical depth χ in a path segment is given by

$$\chi_{ext} = \int \sigma_{ext}\, ds \quad (26)$$

$$\chi_{ext} = \int \left(\frac{\sigma_{ext}}{\rho}\right) \rho\, ds \quad (27)$$

$$\chi_{ext} \equiv \int v_{ext} \rho\, ds \quad (28)$$

6.3. Molecular continua

In addition to their normal HITRAN line contributions, additional 'continuum' features are required to fully model the absorption of several molecules, as listed in Table 3.

The CO_2 and H_2O continua can be thought of as a combination of the accumulation of line wings beyond the $\pm 25\ cm^{-1}$ truncation plus non-Voigt effects. For CO_2 continuum, the non-Voigt effect is represented by the application of the χ-factor (Section 6.5). The MT_CKD definition of the H_2O continuum requires a modification of the H_2O line shape calculation: the value of the Lorentz line shape evaluated at $25\ cm^{-1}$ from line-centre has to be subtracted from each line as this is included in the continuum.

The O_2 and N_2 continua are collision-induced effects which could, in principle, also be represented by Collision-Induced Absorption data (Section 6.6).

6.4. Line mixing

Line-mixing is non-linear effect where the absorption cross-section cannot be simply represented as the summation of individual lineshapes. It particularly affects spectral regions containing many strong overlapping lines such as the Q-branches of CO_2 and, to a lesser extent, CH_4.

The RFM uses the 1st-order model of Strow et al. [28] to model line-mixing in the CO_2 15 and 4.3 μm bands. This adds a significant computational overhead.

6.5. Chi-factor

CO_2 lines are observed to have a narrower width than predicted by the conventional Voigt lineshape. This can be modelled in the RFM using the correction factor of Cousin et al. [6]. This also adds a significant computational overhead.

6.6. Collision-induced absorption

A relatively new addition to HITRAN is a set of files tabulating collision-induced absorption cross-sections [23]. These differ from other absorption cross-section data in that they depend on the combined concentrations of both molecules involved in the collisions. These are not included in the RFM by default but can be added as an option.

These data include alternative representations of the infrared continua of O_2 and N_2 (Section 6.3) although, at the time of writing, lack the necessary O_2–N_2 terms to represent the behaviour of these continua in air rather than as samples of pure O_2 or N_2.

6.7. Look-up tables

The RFM has the capacity to generate and use tabulations of absorption coefficient $k(\nu, p, T, e)$ [see associated paper submitted to JQSRT].

These can be used as an alternative to either line or cross-section data, although the main advantage is the speed saving compared to line-by-line calculations, although at the expense of some interpolation error and large files.

6.8. Surface effects

By default the RFM assumes that the surface is a black body (emissivity = 1) with temperature matching the lowest temperature in the atmospheric profile. However, both surface temperature and (spectral) emissivity can be altered via the driver table. If the surface emissivity is less than unity a specularly reflected path is also modelled (3rd and 4th terms in Eq. (14)).

Jacobian spectra can also be calculated for perturbations in surface temperature and emissivity.

The RFM contains no solar term but the net reflected solar radiance reaching the observer can be obtained from a multiplication of a user-supplied solar source function with the RFM calculation of reflected path transmittance (the term $(1-\epsilon)\tau_{atm}^2$ in Eq. (14)).

Table 3
Molecular continua modelled in the RFM.

Molecule	Spectral range (cm^{-1})	Source
H_2O	0–20 000	MT_CKD_2.5 [21]
CO_2	0–4000	GENLN2 [9]
O_2	1365–1800	Thibault et al. [30]
N_2	2125–2600	Lafferty et al. [18]

6.9. Spectral convolution

The RFM default output is monochromatic spectra at the user-defined spacing. As mentioned in Section 4.3 a fine grid is required to capture the full spectral structure.

However, the RFM can also generate output spectra which represent a convolution of these monochromatic spectra to a lower resolution, equivalent to the effect of an (apodised) instrument line shape (ILS) for Fourier transform spectrometers. With an ILS function ψ, the measured radiance at nominal wavenumber ν is given by

$$R(\nu) = \int L(\nu')\psi(\nu' - \nu)\, \mathrm{d}\nu' \tag{29}$$

To simulate this the RFM performs an internal high spectral resolution calculations on a fine grid (default spacing 0.0005 cm^{-1}), and convolves these with user-supplied ILS function interpolated to the same grid $\Psi_i = \psi(\nu_i - \nu)$:

$$R(\nu) \simeq \left(\frac{1}{\sum_{i=1}^{n} \Psi_i}\right) \sum_{i=1}^{n} L(\nu_i)\Psi_i \tag{30}$$

The half-width of Ψ_i is limited to 1 cm^{-1} by the internal grid (Section 4.3): during the finemesh pass, spectral data is only retained internally from the current and previous 1 cm^{-1} intervals, thus limiting the maximum range over which the convolution can be applied. For wider ILS functions (e.g., unapodised) it is necessary to output the full high resolution spectrum and perform the convolution externally.

The RFM also has its own, implicit triangular ILS function which provides a simple way to generate spectrally averaged output at lower resolutions without specifying an ILS function. For example, spectra can be output at 0.1 cm^{-1} intervals where each point represents a triangularly weighted averaging of monochromatic spectra between the output grid points.

6.10. Field-of-view convolution

A real instrument convolves the incoming radiance with its field-of-view (or point spread function) ϕ. For limb-viewing, assuming radiance only varies significantly in the vertical/elevation direction, the measured radiance R at nominal tangent height z is given by

$$R(z) = \int L(z')\phi(z' - z)\, \mathrm{d}z' \tag{31}$$

For the RFM, the user supplies a representation of the FOV function Φ_i tabulated at $n \geq 3$ arbitrarily spaced points relative to the nominal tangent height. In principle this is the same as the spectral convolution but in this case there is no fundamental 'fine' altitude grid on which to interpolate. Instead the RFM calculates 'pencil-beam' radiances for each path represented by the tabulated points and then combines these according to

$$R(z) \simeq \left(\frac{1}{\sum_{i=1}^{n} a_i}\right) \sum_{i=1}^{n} a_i L(z_i) \tag{32}$$

$$a_i = \frac{\Phi_{i-1}}{z_i - z_{i-1}} + 4\frac{\Phi_i}{z_{i+1} - z_{i-1}} + \frac{\Phi_{i+1}}{z_{i+1} - z_i} \tag{33}$$

This is equivalent to an integration assuming that both the radiance field L and FOV function ϕ vary linearly between tabulated points.

Atmospheric limb radiance usually has a maximum variation with height in the optically thin limit, where it varies approximately proportional to tangent point density, i.e., with a scale height of about 7 km. Thus, unless attempting to model smaller scale structures such as clouds, gravity waves, or VMR profiles with a steep gradient, sampling at 1 km intervals is generally adequate.

6.11. Jacobians

Jacobian spectra are defined as the derivative of the nominal spectra with respect to some perturbation in the atmospheric profile or surface parameters. Profile perturbations can either be at specific levels or a scaling of the whole profile itself ('column' perturbation).

Jacobian spectra are calculated numerically, i.e., the RFM applies a small perturbation, calculates new spectra, and takes the difference with respect to the unperturbed spectra. However, since each perturbation only generates a small number of new path segments (at the perturbed level), the increase in time required for a full set of perturbations at n profile levels is approximately a factor 2 rather than a factor n.

6.12. 2-D atmosphere

For the limb-viewing geometry it is also possible to define a 2-D atmosphere by specifying different atmospheric profiles in the line-of-sight direction using an extra coordinate ϕ, the angle subtended at the centre of curvature (for example, equivalent to latitude if viewing meridionally).

The main consequence is for the ray tracing, which then has to satisfy [24]:

$$\frac{\mathrm{d}r}{\mathrm{d}s} = \cos\theta \tag{34}$$

$$\frac{\mathrm{d}\phi}{\mathrm{d}s} = \frac{\sin\theta}{r} \tag{35}$$

$$\frac{\mathrm{d}\theta}{\mathrm{d}s} = -\sin\theta\left[\frac{1}{r} + \frac{1}{n}\left(\frac{\mathrm{d}n}{\mathrm{d}r}\right)_{\phi}\right] + \frac{\cos\theta}{nr}\left(\frac{\partial n}{\partial \phi}\right)_r \tag{36}$$

These are integrated numerically with a 4th order Runge–Kutta scheme (see, for example, [22]).

6.13. Non-LTE

The default assumption, of local thermodynamic equilibrium (LTE), is that the kinetic temperature, related to the root-mean-square velocity of the molecules, can also describe the population distributions of the internal vibrational and rotational levels of the molecules using Boltzmann statistics. This assumes the time between collisions, which serve to redistribute energy thus maintaining the equilibrium, is much shorter than the natural lifetime of excited states. A consequence is that the Planck function can be used as the source function in the radiative transfer equations (Eqs. (13), (14)).

This is generally a good approximation for much of the infrared (and longer wavelengths) below the stratopause. At higher altitudes, or shorter wavelengths, and where excitation from solar radiation becomes significant, the population distribution among the vibrational levels can become significantly distorted ('non-LTE').

The RFM can model such effects with 'vibrational temperature' profiles specific to each affected molecule, isotopic variation and vibrational level, following the method of Edwards et al. [10], with consequent modifications to the radiative transfer equations.

It is emphasised that the RFM does not itself calculate the vibrational level populations; these have to be supplied by the user, generally from a dedicated non-LTE model.

6.14. B linear in χ

Clough et al. [3] pointed out that the assumption that the effective emitting temperature of a layer (Section 5.4) can be equated to the CG equivalent temperature only applies to optically thin layers. For a spectral region where the layer is optically thick the effective emitting level moves towards the observer.

They suggested modelling this for plane-parallel atmospheres by assuming that the Planck function B varies linearly through the layer with optical depth χ, with the CG temperature used as the asymptotic limit for low optical thickness.

This model, with an equivalent expression for limb-viewing, can be invoked within the RFM simply by setting a flag in the driver file.

6.15. Flux calculations

So far all discussion has referred to line-of-sight radiances, defined per unit solid angle.

For the plane parallel atmosphere, the RFM can also perform a hemispheric integration using the Gaussian quadrature method suggested by Clough et al. [3]. Surface reflections are treated as Lambertian rather than specular.

Additional output spectra associated with such calculations are inter-level transmittances (Curtis Matrices) and cooling rates.

6.16. Rayleigh extinction

The RFM can simulate extinction due to Rayleigh scattering, i.e., the reduction in amplitude at short wavelengths due to molecular scattering out of the line-of-sight beam.

The 'scattering' in this case is simulated as an 'absorption' feature of air, following the algorithm of Bodhaine et al. [1]. Unlike other absorption features, this depends on the density and composition of air which, in the absence of any specific user-profiles, are assumed to have standard concentrations of nitrogen, oxygen, carbon-dioxide and argon.

7. Other applications

7.1. Microwave calculations

The basic radiative transfer for the microwave region ($\nu \sim 10\,\mathrm{cm}^{-1}$) is the same as for the infrared ($\nu \sim 1000\,\mathrm{cm}^{-1}$) but with a few modifications to the default operation (the generation of Rayleigh–Jeans brightness temperatures was covered in Section 6.1).

Firstly, the Van Vleck–Weisskopf correction to the Voigt lineshape theoretically gives a better fit for the pressure-broadened component (effectively incorporating the wings of the 'image' line centred at $-\nu_0$).

Secondly, since the Doppler width scales as wavenumber, a much finer grid than $0.0005\,\mathrm{cm}^{-1}$ is required to capture structure in limb spectra.

These adjustments can simply be applied via the driver table.

However, the RFM refraction calculation (Section 3.3) includes no water-vapour dependence and that the H_2O continuum is only crudely represented at a $10\,\mathrm{cm}^{-1}$ ($\sim$300 GHz) intervals. For these, the source code would have to be altered to introduce microwave-specific models.

Table 4
Default (terrestrial) values of adjustable RFM parameters.

Symbol	Value	Description	Application
r_E	6367.421 km	Radius of curvature	Ray-tracing in circular geometry
g	$9.80665\,\mathrm{m\,s}^{-2}$	Gravitational acceleration	Hydrostatics in planar geometry
M_{air}	$28.964\,\mathrm{kg\,kmol}^{-1}$	Molar mass of air	Hydrostatics in planar geometry
C_p	$29012.0\,\mathrm{J\,K}^{-1}\,\mathrm{kmol}^{-1}$	Molar heat capacity of air	Cooling rate
T_{sp}	2.7 K	Cosmic background temperature	Microwave calculations

7.2. Extra-terrestrial atmospheres

The atmospheric profile within the RFM is entirely user-specified so the main adaptation for a non-terrestrial atmosphere is straightforward.

However, depending on the type of calculation, there are other parameters for which the RFM assumes, by default, terrestrial values (Table 4), all of which can be altered via the driver file.

The radius of curvature is perhaps the most obviously Earth-specific parameter. This is required for ray-tracing in the circular geometry (Section 3.2), e.g., for limb-viewing.

For plane-parallel atmospheres, the conversion from altitude to pressure for the CG integration (Section 3.1) assumes hydrostatic equilibrium and therefore requires values for gravitational acceleration and the molar mass of air (although the hydrostatic assumption itself can be over-ridden via the driver file).

Cooling rate calculations (Section 6.15) are, effectively, a conversion from radiation loss to temperature change for an atmospheric layer, and therefore require some value of heat capacity.

The cosmic background temperature is used to calculate the Planck function representing cold space, B_0, in Eqs. (13) and (14). By its very definition it is not specific to the Earth, but is included here since it can be adjusted in the same way as the other parameters.

Strictly speaking, the RFM refraction (Section 3.3) and Rayleigh extinction (Section 6.16) modules are also Earth-specific, but these are primarily dependent upon molecular number density rather than detailed composition, so should be adequate for other atmospheres.

The RFM aside, it should be remembered that most spectroscopic data are also intrinsically terrestrial, e.g., HITRAN line broadening parameters are defined for air rather than, say hydrogen or methane.

7.3. Visible and ultraviolet

The lack of any scattering or solar component limits the RFM's usefulness for radiative transfer at short wavelengths. However, it can still be used to model molecular absorption using the HITRAN line and cross-section data (which extend to UV wavelengths). Also, Rayleigh extinction (Section 6.16) can be used to model scattering out of a beam.

8. Conclusions

The RFM is a general purpose radiative transfer model that has been widely used for 20 years. In that time it has continued to evolve and, inevitably, this paper just summarises its current state (v4.34).

Some anticipated future developments are as follows:

1. Conversion to Fortran90/95, mainly for the dynamic array sizing and complex matrix operations
2. Incorporation of more sophisticated CO_2 and CH_4 line-mixing algorithms, although their structure (requiring all lines within a band to be considered simultaneously) does not fit in easily within the RFM line-by-line approach
3. Include single-scattering, using a combination of the line-of-sight and hemispherically averaged (flux) calculations
4. More sophisticated treatment of surface reflections, e.g., a Lambertian as well as a specular component, also with a combination of line-of-sight and flux calculations
5. Allow for extra lineshape parameters, following the recommendations of Tennyson et al. [29], assuming these parameters become available in the on-line HITRAN.

Acknowledgements

The RFM was originally developed under ESA contract PO-SW-ESA-GS-00323 (1995). Maintenance and development are currently supported by the National Centre for Earth Observation. I would also like to thank the many users who have helped to improve the code by reporting bugs.

References

[1] Bodhaine Barry A, Wood Norman B, Dutton Ellsworth G, Slusser James R. On Rayleigh optical depth calculations. J Atmos Ocean Technol 1999;16:1854–61.
[2] Bormann N, Healy SB. A fast radiative-transfer model for the assimilation of MIPAS limb radiances: accounting for horizontal gradients. Q J R Meteorol Soc 2006;132(October (620)):2357–76.
[3] Clough Shepard A, Iacono Michael J, Moncet Jean-Luc. Line-by-line calculations of atmospheric fluxes and cooling rates: application to water vapor. J Geophys Res: Atmos 1992;97(D14):15761–85.
[4] Collins WD, Ramaswamy V, Schwarzkopf MD, Sun Y, Portmann RW, Fu Q, et al. Radiative forcing by well-mixed greenhouse gases: estimates from climate models in the intergovernmental panel on climate change (IPCC) fourth assessment report (AR4). J Geophys Res 2006;111(D14).
[5] Costa SMS, Shine KP. An estimate of the global impact of multiple scattering by clouds on outgoing long-wave radiation. Q J R Meteorol Soc 2006;132(April (616)):885–95.
[6] Cousin C, Le Doucen R, Boulet C, Henry A. Temperature dependence of the absorption in the region beyond the4.3-μm band head of CO_2. 2: N_2 and O_2 broadening. Appl Opt 1985;24(November (22)): 3899–907.
[7] Dudhia Anu. Reference forward model; 2016.
[8] Dudhia Anu, Morris Paul E, Wells Robert J. Fast monochromatic radiative transfer calculations for limb sounding. J Quant Spectrosc Radiat Transf 2002;74(6):745–56.
[9] Edwards David P. Genln2: a general line-by-line atmospheric transmittance and radiance model, version 3.0 description and users guide. Technical report NCAR/TN-367+STR, NCAR; 1992.
[10] Edwards David P, Lpez-Puertas Manuel, Lpez-Valverde Miguel A. Non-local thermodynamic equilibrium studies of the 15-m bands of CO_2 for atmospheric remote sensing. J Geophys Res: Atmos 1993;98 (D8):14955–77.
[11] Ewen GBL, Grainger RG, Lambert A, Baran AJ. Infrared radiative transfer modelling in a 3D scattering cloudy atmosphere: application to limb sounding measurements of cirrus. J Quant Spectrosc Radiat Transf 2005;96(1):45–74.
[12] Fischer H, Birk M, Blom C, Carli B, Carlotti M, von Clarmann T, et al. Mipas: an instrument for atmospheric and climate research. Atmos Chem Phys 2008;8(8):2151–88.
[13] Fischer J, Gamache RR, Goldman A, Rothman LS, Perrin A. Total internal partition sums for molecular species in the 2000 edition of the {HITRAN} database. J Quant Spectrosc Radiat Transf 2003;82(1–4):401–12. The {HITRAN} Molecular Spectroscopic Database: Edition of 2000 Including Updates of 2001.

[14] Glatthor Norbert, Hoepfner Michael, Stiller Gabriele P, von Clarmann Thomas, Dudhia Anu, Echle Georg, et al. Intercomparison of the kopra and the rfm radiative transfer codes. Proc SPIE 1999; 3867: 348-363.
[15] Illingworth SM, Remedios JJ, Boesch H, Moore DP, Sembhi H, Dudhia A. Ulirs, an optimal estimation retrieval scheme for carbon monoxide using iasi spectral radiances: sensitivity analysis, error budget and simulations. Atmos Meas Tech 2011;4(2):269–88.
[16] Jacquinet-Husson N, Crepeau L, Armante R, Boutammine C, Chdin A, Scott NA, et al. The 2009 edition of the {GEISA} spectroscopic database. J Quant Spectrosc Radiat Transf 2011;112(15):2395–445.
[17] Kaye GWC, Laby TH. Tables of physical and chemical constants. 16th ed. London: Longman; 1995.
[18] Lafferty Walter J, Solodov Alexander M, Weber Alfons, Olson Wm Bruce, Hartmann Jean-Michel. Infrared collision-induced absorption by N_2 near 4.3 μm for atmospheric applications: measurements and empirical modeling. Appl Opt 1996;35(October (30)):5911–7.
[19] Line Michael R, Zhang Xi, Vasisht Gautam, Natraj Vijay, Chen Pin, Yung Yuk L. Information content of exoplanetary transit spectra: an initial look. Astrophys J 2012;749(1):93.
[20] Lpez-Valverde MA, Lpez-Puertas M, Lpez-Moreno JJ, Formisano V, Grassi D, Maturilli A, et al. Analysis of non-lte emissions at in the martian atmosphere as observed by pfs/mars express and sws/iso. Planet Space Sci 2005;53(10):1079–1087. First Results of the Planetary Fourier Spectrometer aboard the Mars Express Mission.
[21] Mlawer Eli J, Payne Vivienne H, Moncet Jean-Luc, Delamere Jennifer S, Alvarado Matthew J, Tobin David C. Development and recent evaluation of the mt_ckd model of continuum absorption. Philos Trans R Soc Lond A: Math Phys Eng Sci 2012;370(1968):2520–56.
[22] Press William H, Teukolsky Saul A, Vetterling William T, Flannery Brian P. Numerical recipes in FORTRAN; the art of scientific computing. 2nd ed.New York, NY, USA: Cambridge University Press; 1993.
[23] Richard C, Gordon IE, Rothman LS, Abel M, Frommhold L, Magnus Gustafsson J-M, et al. New section of the HITRAN database: collision-induced absorption (cia). J Quant Spectrosc Radiat Transf 2012;113(11):1276–85.
[24] Rodgers Clive D. Inverse methods for atmospheric sounding, theory and practice. Singapore: World Scientific; 2000.
[25] Rothman LS, Gordon IE, Babikov Y, Barbe A, Chris Benner D, Bernath PF. The {HITRAN2012} molecular spectroscopic database. J Quant Spectrosc Radiat Transf 2013;130:4–50 [{HITRAN2012} special issue].
[26] Rothman LS, Rinsland CP, Goldman A, Massie ST, Edwards DP, Flaud J-M, et al. The HITRAN molecular spectroscopic database and hawks (HITRAN atmospheric workstation): 1996 edition. J Quant Spectrosc Radiat Transf 1998;60(5):665–710.
[27] Saunders R, Rayer P, Brunel P, von Engeln A, Bormann N, Strow L, et al. A comparison of radiative transfer models for simulating atmospheric infrared sounder (airs) radiances. J Geophys Res: Atmos 2007;112(D1):n/a–n/a, D01S90.
[28] Larrabee Strow L, Tobin David C, Hannon Scott E. Special issue atmospheric spectroscopy applications a compilation of first-order line-mixing coefficients for CO_2Q-branches. J Quant Spectrosc Radiat Transf 1994;52(3):281–94.
[29] Tennyson Jonathan, Bernath Peter F, Campargue Alain, Császár Attila G, Daumont Ludovic, Gamache Robert R, et al. Recommended isolated-line profile for representing high-resolution spectroscopic transitions (IUPAC technical report). Pure Appl Chem 2014;86(January (12)).
[30] Thibault F, Menoux V, Le Doucen R, Rosenmann L, Hartmann J-M, Boulet Ch. Infrared collision-induced absorption by O_2 near 6.4 μm for atmospheric applications: measurements and empirical modeling. Appl Opt 1997;36(January (3)):563–7.
[31] Tjemkes SA, Patterson T, Rizzi R, Shephard MW, Clough SA, Matricardi M, et al. The {ISSWG} line-by-line inter-comparison experiment. J Quant Spectrosc Radiat Transf 2003;77(4):433–53.
[32] Ungermann J, Kaufmann M, Hoffmann L, Preusse P, Oelhaf H, Friedl-Vallon F, et al. Towards a 3-D tomographic retrieval for the airborne limb-imager GLORIA. Atmos Meas Tech 2010;3(November (6)):1647–65.
[33] von Clarmann T. Intercomparison of radiative transfer codes under non-local thermodynamic equilibrium conditions. J Geophys Res 2002;107(D22).
[34] Wells RJ. Rapid approximation to the Voigt/Faddeeva function and its derivatives. J Quant Spectrosc Radiat Transf 1999;62(1):29–48.
[35] Wooster MJ, Freeborn PH, Archibald S, Oppenheimer C, Roberts GJ, Smith TEL, et al. Field determination of biomass burning emission ratios and factors via open-path ftir spectroscopy and fire radiative power assessment: headfire, backfire and residual smouldering combustion in African Savannahs. Atmos Chem Phys 2011;11(22): 11591–615.